V European Conference on Computational Fluid Dynamics
ECCOMAS CFD 2010
J. C. F. Pereira and A. Sequeira (Eds)
Lisbon, Portugal,14-17 June 2010

NUMERICAL MODELING OF VORTICITY DYNAMICS IN OCEANIC WAKES

Dmitri Boutov[†], Aires Santos[††], Euclides Luís[*,] and Juha H. Videman[‡]**

[†]Institute of Oceanography, Faculty of Sciences, University of Lisbon,
Campo Grande, 1749-016, Lisboa, Portugal
e-mail: dboutov@fc.ul.pt
[††]Department of Mechanical Engineering/MARETEC, Instituto Superior Técnico
Av. Rovisco Pais, 1049-001 Lisboa, Portugal
e-mail: aires.santos@ist.utl.pt
[*]Department of Basic Sciences, Faculty of Engineering, Agostinho Neto University,
Av. 21 de Janeiro, Luanda, Angola
[**]Center for Mathematics and its Applications (CEMAT), Instituto Superior Técnico,
Av. Rovisco Pais, 1049-001 Lisboa, Portugal
e-mail: eluis@math.ist.utl.pt
[‡]Department of Mathematics/CEMAT, Instituto Superior Técnico,
Av. Rovisco Pais, 1049-001 Lisboa, Portugal
e-mail: videman@math.ist.utl.pt

Key words: oceanic wakes, ROMS, vorticity dynamics, cyclonic-anticyclonic asymmetries

Abstract. *Numerical simulations were performed using the ROMS ocean model in a fluid domain containing an obstacle with the Madeira island contour. Both stratification and rotation effects were taken into account. The results suggest the existence of an asymmetric island wake with stronger cyclones than anticyclones. Contrary to the simulations conducted around a circular island, no values of the dimensionless parameters were found to lead to symmetric wake dynamics or to a regime with anticyclonic eddy dominance.*

1 INTRODUCTION

This study aims at widening our understanding of deep-water island wakes. Satellite observations have revealed the formation of spectacular vortex streets in the wakes behind islands and a great effort has been made to understand this physical process [1, 2, 3, 4, 5, 6, 7] as well has its biological and environmental impact [8, 9, 10, 11, 12, 13].

A classical example of an oscillatory wake pattern behind an obstacle is the periodic vortex shedding in a uniform flow past a circular cylinder. This regular, periodic shedding, referred to as the Kármán vortex street, is well characterized by the Reynolds number Re (the ratio of inertial forces to viscous forces) defined by

$$Re = \frac{UL}{\nu_m}\,, \tag{1}$$

where U is the unperturbed upstream velocity, L the horizontal length scale of the obstacle and ν_m the kinematic (molecular) viscosity of the fluid.

In geophysics, rotation and stratification distinguish the three-dimensional wakes from the classical non-rotating, homogeneous wakes and other dimensionless parameters come into play. The relevant parameters for the analysis of oceanic wakes are the Reynolds number, the Rossby number Ro (the ratio of inertial forces to Coriolis forces)

$$Ro = \frac{U}{fL}\,, \tag{2}$$

and the Froude number Fr (the ratio of inertial forces to buoyancy forces)

$$Fr = \frac{U}{NH}\,, \tag{3}$$

Here, H is the vertical scale of the fluid domain, f the Coriolis frequency and

$$N = \sqrt{-\frac{g}{\rho_0}\frac{\partial \rho}{\partial z}}\,, \tag{4}$$

the Brunt-Väisälä frequency (ρ and ρ_0 are the fluid density and the constant mean density, respectively, and g the acceleration due to gravity). The Burger number Bu is defined as

$$Bu = \left(\frac{Ro}{Fr}\right)^2\,, \tag{5}$$

or, equivalently

$$Bu = \left(\frac{NH}{fL}\right)^2 = \left(\frac{R_d}{L}\right)^2\,, \tag{6}$$

where R_d is the baroclinic deformation radius, and the Strouhal number St by

$$St = \frac{L}{UT}\,. \tag{7}$$

In the classical nonrotating, unstratified flow, there is no boundary layer separation and therefore no wake if $Re \ll 1$ or $Re \to \infty$, in the former case because the viscous forces dissipate any perturbation and in the latter because the flow behaves as if it were inviscid. The wake does occur in the range $10^2 < Re < 10^7$, with an average Strouhal number $St \approx 0.2$, cf. White [14], that is, the stronger the velocity of the uniform flow or the smaller the diameter of the cylinder, the greater the frequency of the eddy shedding. In geophysical flows, increasing rotation (decreasing Ro) tends to inhibit vortex shedding. On the other hand, strengthening density stratification (decreasing Fr) suppresses vertical motion and the vortex shedding tends to occur at lower Reynolds numbers than in more weakly stratified flows.

Another distinctive feature in oceanic wakes is the centrifugal instability, also known to as the inertial instability, cf. [15]. The classical wakes are symmetric, with clockwise and anticlockwise vortices spinning around with more or less same magnitude, but in geophysical flows the anticyclonic eddies lose their strength (in the Northern Hemisphere) if $|\zeta| > f$, with $\zeta = \partial v/\partial x - \partial u/\partial y$ denoting the vertical component of the relative vorticity, which is a manifestation of centrifugal instability. This also means that increasing the Rossby or Reynolds number (within the range where the vortex shedding occurs), makes the cyclonic eddies more pronounced.

Given that the wake is a highly unstable fluid region, it is necessary to distinguish between the barotropic and baroclinic instabilities. In general, the problem is purely baroclinic only when the horizontal scale of the undisturbed flow is large compared to the baroclinic deformation radius, i.e., when $Bu \ll 1$. In this case, the available energy in the undisturbed flow is mainly potential. The opposite, purely barotropic, limit occurs when the vertical variations of the velocity can be neglected. In most cases of practical interest, there exists a mixture of both baroclinic and barotropic effects, cf. [16].

In this paper, we present our recent results on deep-water island wakes, that is, wakes wherein the dominant boundary stress is associated with the lateral side of the island rather than the nearshore bottom. The main emphasis lies on the comparison between a symmetric, circular island, see [7], and a non-symmetric one with the Madeira island contour. As in [7], the island is assumed to be a vertical cylinder and the ocean bottom flat.

Madeira archipelago, located at about 33°N and 17°W, is a group of deep-sea islands located in NE Atlantic, consisting of the islands of Madeira, Porto Santo, Desertas and Selvagens. Our study region is centred in the waters around Madeira, the main island of the Madeira archipelago. Madeira has a maximum length of about 50 km in the East-West direction and 20 km in the North-South direction. Its obstruction to the incoming oceanic and atmospheric flows induces leeward wake instabilities, which have been observed both by remote sensing and field data [6].

2 NUMERICAL SETUP

The numerical model Regional Ocean Modeling System (ROMS) is applied in the 300 km wide (East-West direction) and 320 km long (North-South direction) computational domain, see Fig. 1. The depth is assumed uniform ($H_m = 500$ m) and the island is placed in a channel-like configuration with prescribed southward inflow and density profiles (in thermal wind balance) at the northern upstream boundary. At the southern outflow boundary, a clamped condition with a sponge layer is used for the velocity and density fields, whereas at the eastern and western boundaries no normal flow boundary conditions apply. No-slip boundary conditions are considered through a land-mask algorithm at the island boundary. At the bottom, the weak horizontal velocities imply a negligible bottom friction in agreement with the deep-water wake hypothesis. The surface stress, heat and freshwater fluxes are set to zero. The initial condition for the velocity matches the upstream boundary condition except at the island points with land masks. The grid spacing is $\Delta x = \Delta y = 1\,\mathrm{km}$ and in the vertical the domain has 20 sigma layers. The total integration time is 100 days with spin-up period of about 20 days.

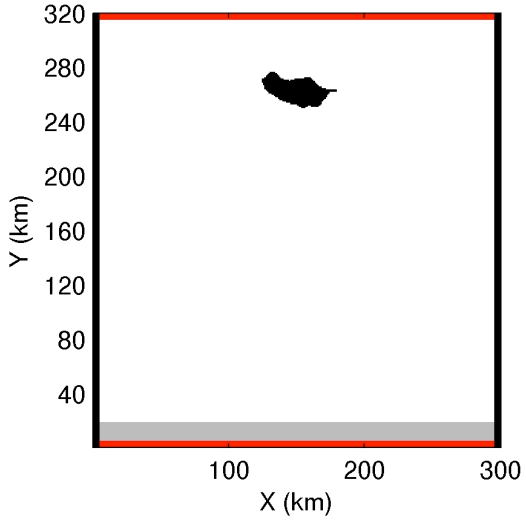

Figure 1: Computational domain. The black and red lines correspond to closed and open boundaries, respectively. The grey area represents the sponge layer.

The incoming meridional velocity profile for $-H_m < z < 0$ is

$$v(z) = v_{m1} - v_{m2} \tanh\left(\frac{z + h_s}{h_d}\right), \tag{8}$$

where $v_{m1} + v_{m2}$ and $v_{m1} - v_{m2}$ are the constant near-surface and bottom currents, respectively, and h_s is the central depth and h_d the mean thickness of the shear layer. The incoming zonal and vertical currents are set to zero. The upstream density and velocity fields are related through the thermal wind equations. Thus

$$\rho(x,z) = \rho_0 + \Delta\rho \ \tanh\left(\frac{z+h_c}{h_t}\right) - \frac{\rho_0 f}{g}\int_{x_0}^{x}\frac{\partial v}{\partial z}\,dx\,, \tag{9}$$

where $x_0 = 150$ km and $\Delta\rho$, h_c and h_t are parameters related to the thermocline (the region with largest density changes); the value of $\Delta\rho$ corresponds to about half of the density change in the thermocline, h_c is the central depth of the thermocline and h_t is its thickness, all chosen subject to the assumption of a stable stratification, i.e. $\partial\rho/\partial z \leq 0$ everywhere in the fluid domain. Considering $v_{m1} = v_{m2} = -0.1$ m/s, $h_s = 120$ m, $h_d = 80$ m, $\Delta\rho = 2$ kg/m^3, $h_c = 125$ m, $h_t = 90$ m and $f = 4.46 \cdot 10^{-5}$ s^{-1}, the vertical profiles of the density anomaly $\sigma = \rho - 1000$ and meridional velocity imposed as inflow conditions at the northern boundary, are represented in Fig. 2.

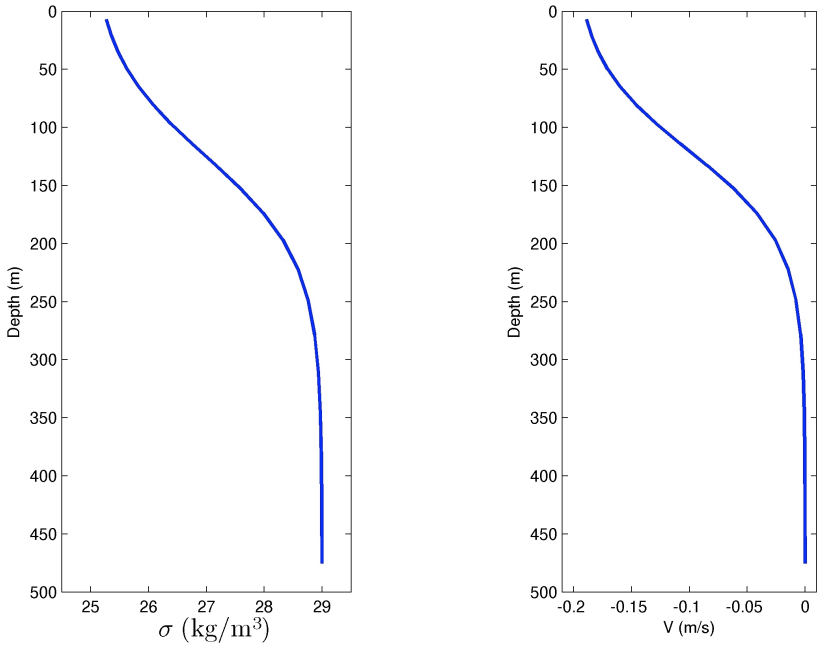

Figure 2: The initial density anomaly at the centre ($x = 150$ km) of the fluid domain (left). The zonally uniform meridional velocity profile (right).

Finally, the initial surface elevation is related to the surface velocity via geostrophic balance

$$\eta(x) = \frac{f\,(x - x_0)}{g}\,v(0)\,, \tag{10}$$

Given that the flow is southward, from (8), (9) and (10) it follows that the isopycnal surfaces have a positive slope and the sea level decreases towards the East.

3 RESULTS

In the numerical simulations, we calculated the Reynolds number using the eddy-viscosity ν_e instead of the molecular viscosity ν_m and considered two different values of the Reynolds number ($Re = 400$ and 1600) and three values of the parameter $\lambda = Ro/Bu$ ($\lambda = 0.077, 0.154$ and 0.308). This resulted to the total number of six simulations.

Figures 3, 4 and 5 represent the normalized relative vorticity ζ/f corresponding to $Re = 400$ and $\lambda = 0.077$, the parallel lines in Fig. 4 and 5 showing the position of the eastern and western boundaries of the island. Cyclones and anticyclones are almost aligned, in contrast to the von Kármán wake theory by which the values $h/a = 0.28$ and $a/L = 5$ predict the ratio $h/L = 1.4$, h being the lateral eddy spacing and a the axial eddy spacing.

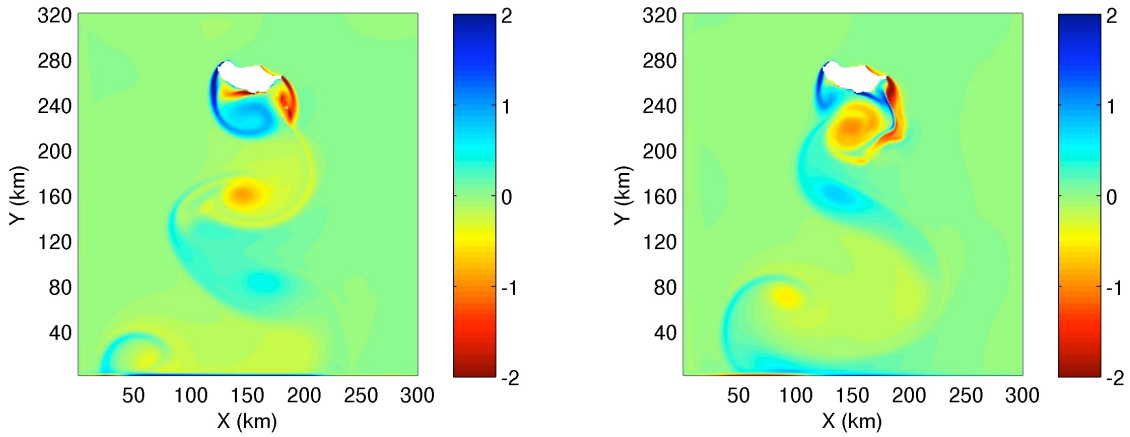

Figure 3: Normalized surface vorticity on day 69 (left) and on day 79 (right).

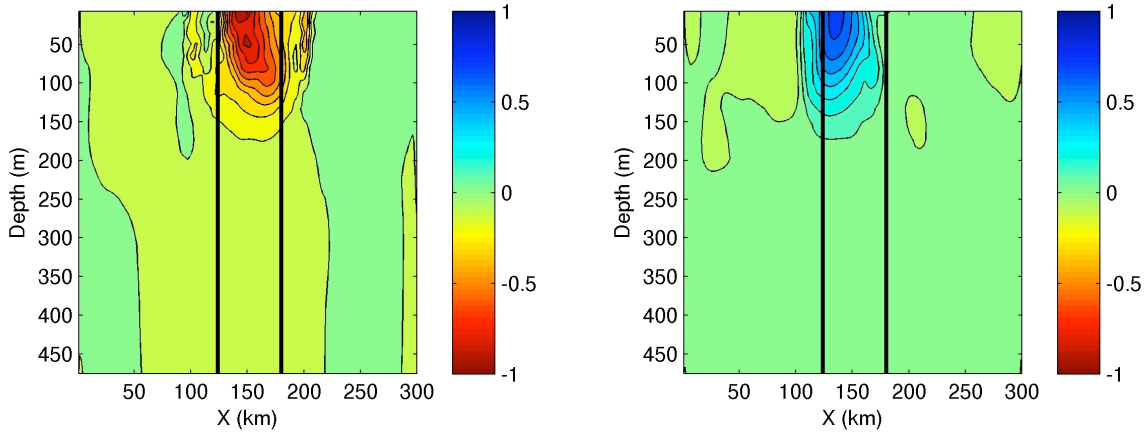

Figure 4: Normalized vorticity at y=160 km on day 69 (left) and on day 79 (right).

From Fig. 5 one can estimate the eddy shedding period T to be approximately 18 days yielding $St \approx 0.18$. This Strouhal number is somewhat lower than the values obtained with a circular cylinder; $St \approx 0.2$ (non-rotating, homogeneous fluid) and $St \approx 0.23$ (considering rotation and stratification and choosing $\lambda = 0.077$, cf. Dong et al. [7]). The lower Strouhal number suggests that this particular island contour inhibits eddy shedding, that is, more time is needed for the vorticity to accumulate in the boundary layer around the island before being advected in the wake.

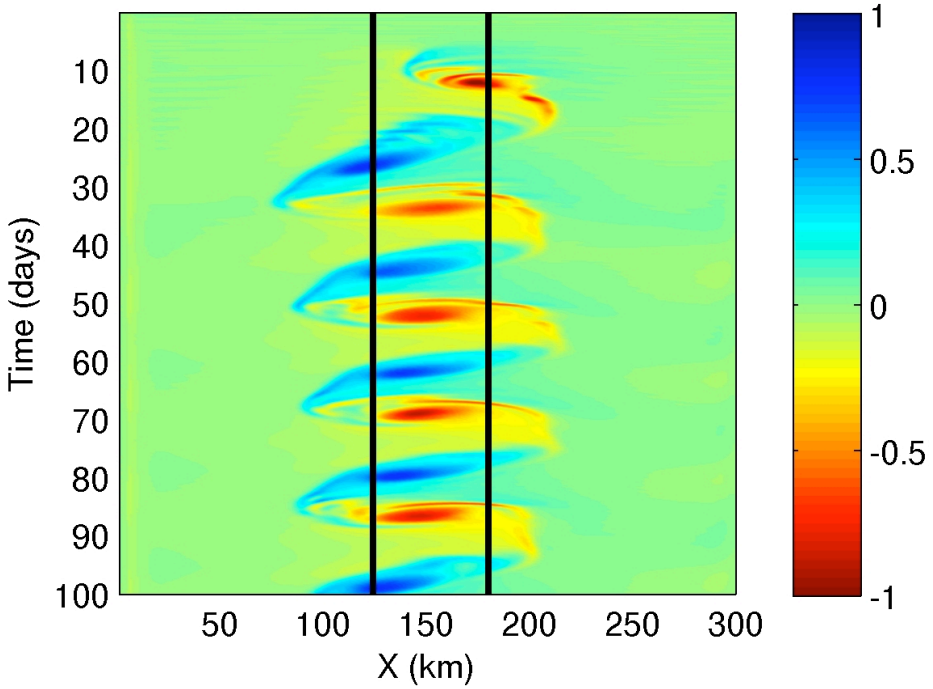

Figure 5: Normalized surface vorticity versus time at y=160km.

To have a quantitative estimate of the wake asymmetry we should look at Fig. 6. This figure represents the normalized mean vorticity difference $\boldsymbol{\zeta} = (|\zeta_-| - \zeta_+)/f$, that is, ζ_- and ζ_+ stand for the negative and positive vorticities averaged over the entire fluid domain during 50 days (from day 50 to day 100). The cyclone predominance is more evident with the higher Re, because of the centrifugal instability. Figure 6 shows also that increasing $\lambda = Ro/Bu$ decreases the wake asymmetry, confirming the results of Perret et al. [17], in particular for $\lambda < 0.15$. This can be explained by the effect of the Burger number Bu, since the increase of relative vorticity related to larger values of Re or Ro, contributes to the centrifugal instability. The Burger number is a measure for barotropic/baroclinic instabilities and from Fig. 6 we conclude that the tendency for the flow to undergo barotropic instability (high Burger number) is related to centrifugal instability. This is not surprising since stronger stratification corresponds to a higher Burger number, cf. (6),

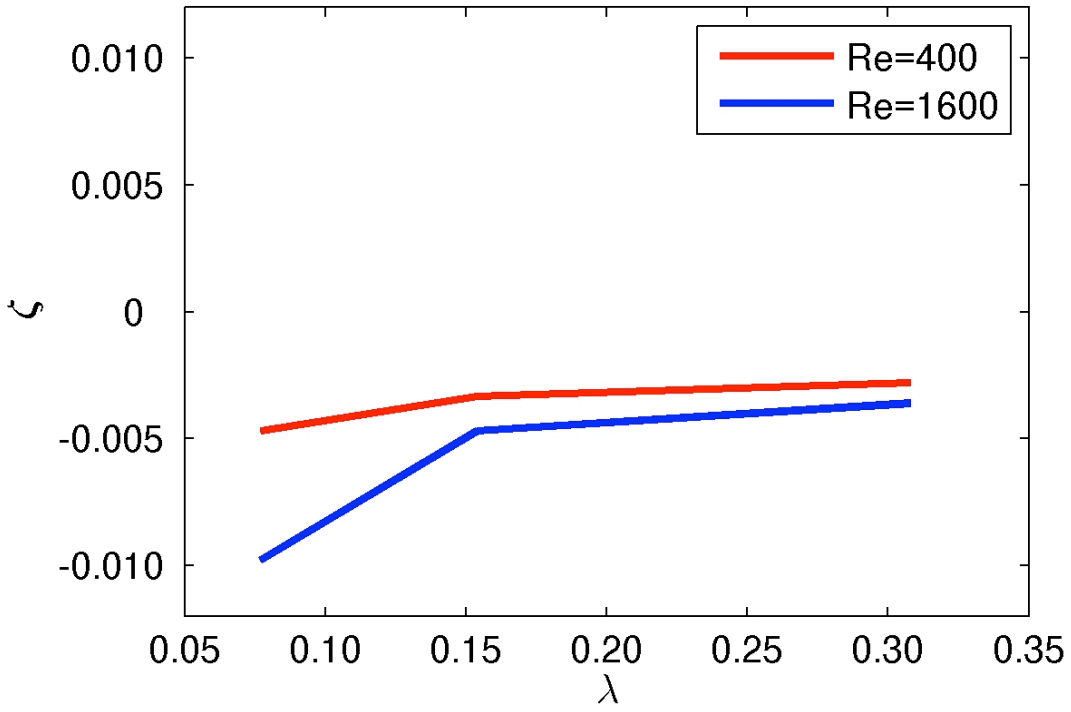

Figure 6: Asymmetry between anticyclonic and cyclonic eddies.

and suppresses vertical motion, more evident when cyclones predominate than in the case where both cyclones and anticyclones have equal strength and vertical velocity, negative in anticyclones and positive in cyclones, becomes an important feature of the flow with major impact on marine life.

4 CONCLUSIONS

This paper presents the results of our simulations of the Madeira island wake obtained by the ROMS numerical model taking into account both the rotation of the Earth and the density stratification of the ocean. Several sensitivity studies were performed changing the values of the Reynolds number Re, the Rossby number Ro and the Burger number Bu. Together they control the three instabilities that may occur in the wake: centrifugal, barotropic and baroclinic. Results were compared with similar simulations around an idealized circular island with the main difference being the predominance of cyclones, regardless of the value of Re, in our case. Contrary to the expectations, cf. Dong et al. [7], no regime of anticyclonic eddy dominance, for moderate values of Re and increasing $\lambda = Ro/Bu$, or dynamical symmetry, for small values of λ, could be found, the only explanation being the particular island contour. As a step closer to reality, future numerical Madeira

island wake simulations should include the real ocean bathymetry, a time varying incoming flow, the effect of the bottom drag on the sloping nearshore topography and the interaction between the oceanic and atmospheric island wakes.

REFERENCES

[1] C. Pattiaratchi, A. James and M. Collins, Island wakes and headland eddies: A comparison between remotely sensed data and laboratory experiments, *J. Geophys. Res.*, **92**, 783–794 (1987).

[2] E. Wolansky and W.M. Hamner, Topographically controlled fronts in the ocean and their biological influence, *Science*, **241**, 177–181 (1988).

[3] J. Aristegui, P. Sangrá, S. Hernandez-Leon, M. Canton, A. Hernandez-Guerra and J. Kerling, Island-induced eddies in the Canary Islands, *Deep-Sea Res. I*, **41**, 1509–1525 (1994).

[4] E. Barton, G. Baxterretxea, P. Flament, E. Mitchelson-Jacob, B. Jones, J. Aristegui and F. Herrera, Lee region of Gran Canaria, *J. Geophys. Res.*, **105**, 17173–17193 (2000).

[5] P. Coutis and J. Middleton, The physical and biological impact of a small island wake in the deep ocean, *Deep-Sea Res. I*, **4**9, 1341–1361 (2002).

[6] R.M.A. Caldeira, S. Groom, P. Miller, D. Pilgrim and N.P. Nezlin, Sea-surface signatures of the island mass effect phenomena around Madeira Island, Northeast Atlantic, *Remote Sense of Environment*, **80**, 336-360 (2002).

[7] C. Dong, J.C. McWilliams and A.F. Shchepetkin, Island Wakes in Deep Water, *J. Phys. Oceanogr.*, **37**, 962–981 (2007).

[8] W.M. Hamner and I.R. Hauri, Effects of island mass: Water flow and plankton pattern around a reef in the Great Barrier Reef lagoon, Australia, *Limnol. Oceanogr.*, **26**, 1084–1102 (1981).

[9] S. Hernandez-Leon, Accumulation of mesozooplankton in a wake area as a causative mechanism of the island-mass effect, *Mar. Biol.*, **109**, 141–147 (1991).

[10] J. Dower, H. Freeland and K. Juniper, A strong biological response to oceanic flow past Cobb seamount, *Deep-Sea Res.*, **39A**, 1139–1145 (1992).

[11] E. Martinez and K. Maamaatuaiahutapu, Island mass effect in the Marquesas Islands: Time variation, *Geophys. Res. Lett.*, **31**, L18307 (2004).

[12] D. Hasegawa, H. Yamazaki, R.G. Lueck and L. Seuront, How islands stir and fertilize the upper ocean, *Geophys. Res. Lett.*, **31**, L16303 (2004).

[13] D. Rissik, I.M. Suthers and C.T. Taggart, Enhanced particle abundance in the lee of an isolated reef in the south Coral Sea: The role of flow disturbance, *J. Plankton Res.*, **19**, 1347–1368 (1997).

[14] F. M. White, Fluid Mechanics, 4th Edition, *McGraw–Hill*, (1998).

[15] J.L. Pelegri, M. Auladell, A.W. Ratsimandresy, P. Sangrá and E. García-Ladona, Inertial instability in oceanic flows, *ERCOTAF Bulletin*, **60**, 22–29 (2004).

[16] A. Gill, Atmosphere-Ocean Dynamics, *Academic Press*, (1982).

[17] G. Perret, A. Stegner, M. Farge and T. Pichon, Cyclone-anticyclone asymmetry of largescale wakes in the laboratory, *Phys. Fluids*, **1**8, 036603 (2006).